

Compact finite difference schemes for soybean hydration model as Stefan problem

Seda Gulen¹ and Turgut Ozis²

¹Department of Mathematics, Namik Kemal University, Tekirdag, Turkey

²Department of Mathematics, Ege University, Izmir, Turkey

Received: 29 September 2017, Accepted: 28 November 2017

Published online: 15 May 2018.

Abstract: In this paper, a study of numerical solutions of a nonlinear soybean hydration model which is considered as a Stefan problem is presented. For this purpose, it is employed fourth and sixth order compact finite difference schemes for discretizing the spatial derivative and the standard finite difference scheme for discretizing the time derivative. To show the efficiency of the methods, numerical experiments have been done and numerical stability has been proven. It is noted that the present methods have more accurate solution with minimal computational effort (CPU time) for soybean hydration model, by comparison of the results in the literature which is validated experimental data.

Keywords: Compact schemes, finite differences, Stefan problem, hydration model.

1 Introduction

Many physical problems arising in engineering and science include volume variation or movement of system boundaries. One of the examples of these problems is diffusion models such as swelling or drying are studied by many authors [1,2,3,4,5,6,7,8]. They have been stated that when the water enters the system, the size of the material increases. Among them, Coutinho [1] has been demonstrated experimentally the increase in volume during the soaking could reach 30% for soybean. This variation is important in modeling the soybean hydration process.

Models that including the hydration of grains are described by empirical models and phenomenological models. Empirical models include simple mathematical correlation but do not describe diffusion steps. In phenomenological models, elementary steps of diffusion and/or convection mass transfer is considered [7] and these models are represented with lumped or distributed parameters. Lumped parameters systems which do not take into account concentration variations inside the grain are modeled by ordinary differential equations. On the other hand, distributed parameter systems represent concentration gradients that change over time inside the grain.

Soybean grains behave as distributed parameter systems whose moisture profiles inside the grain changes over time and can be predicted by phenomenological mathematical models. Since these problems are time-dependent problems, they are modeled by the parabolic partial differential equation with an initial condition and two boundary conditions, are class of initial- boundary value problems. Boundary conditions are adopted for the center and the surface of the grain. In these problems, an additional condition can be adapted for movement of the radius, is the moving boundary, is determined as part of the solution. The behavior of volume increase is described by a differential equation which represents the rate of growth of the radius. Hence, the problem has physical meaning. These problems are called Stefan Problem or moving boundary problems.

Due to difficulties in obtaining the analytical solution of Stefan problems many authors have been dedicated to numerical solutions of Stefan problem by applying various numerical methods including finite differences, finite elements and integral methods. Earlier studies can be found in Ref.[9].

Very recently, Sadoun et al. [10] proposed a modified variable space grid method for heat conduction problem and compared their solution with other solutions in the literature. Yiğit [11] used finite difference method with variable space grid and variable time step for one-dimensional solidification problem to the position of the moving front and its velocity. Also, he developed an analytical method for limiting case and compared with numerical results. Reutskiy [12, 13] presented a new meshless method for one dimensional Stefan problem and Stefan type problem with moving boundaries in spherical coordinates. Mitchell et al.[14] used the Keller box finite difference method with boundary immobilization method for the Stefan problem of evaporation of spherical droplets. Lee et al. [15] proposed a finite difference moving mesh method for moving boundary solution and apply their method to the porous medium equation, Richard's equation and the Crank-Gupta problem.

The swelling problems as Stefan Problem were taken into account by Davey et al.[4], McGuinness et al.[5] and Barry and Caunce [6]. They proposed the moisture diffusion model whose diffusivity is an exponential function of moisture content. In these papers, the models include two moving boundaries simultaneously. One of them expresses the movement of the radius and other expresses the movement of the water inside the material. These studies propose the exact solution for the model but they do not extend to analyzing moisture profiles obtained during modeling.

Viollaz et al.[16] and Viollaz and Rovedo [17] used boundary immobilization method for the problem with volume change due to drying or swelling.

Nicolin et al.[3] present a model with volume variation to analyzes the moisture profiles inside the grain. The model has one moving boundary which represents the behavior of the grain by a differential equation which is named Stefan condition. They solved the problem by explicit finite difference method by validating experimental data.

In this work, it is studied to apply variable space grid method combined with fourth and sixth order compact finite difference method to obtain the solution of the soybean hydration model proposed by Nicolin et al.[3]. The aim is to show that compact finite difference schemes which utilized for soybean hydration model have less computational effort (CPU time) with less iteration to reach the more accurate solutions. Numerical results are compared with Nicolin et al.[3] and computational times and equilibrium times for the proposed models are calculated.

The rest of the paper is as follows: In Section 2, the mathematical model of soybean hydration process is introduced. In Section 3, fourth and sixth order compact finite difference methods are summarized. In Section 4, variable space grid method is applied to the problem and numerical algorithm is described for fourth and sixth order compact finite difference methods. Numerical stability is proven in Section 5 and computational results are given in Section 6 to show the efficiency of the method on the problem. Paper is concluded in Section 7.

2 Mathematical modeling

The model is obtained by transient mass balance on differential volume element of soybean grains. Since the geometry of soybeans is assumed spherical, the Eq.(1) that represent water absorption by soybean is developed in spherical coordinates based on Fick's Law of Diffusion. It is assumed that diffusion takes place only in radial direction.

$$\frac{\partial X}{\partial t} = D \left(\frac{2}{r} \frac{\partial X}{\partial r} + \frac{\partial^2 X}{\partial r^2} \right), \quad (1)$$

where X represents moisture content, r is the radial position which is a function of time and D is the constant diffusion coefficient.

Eq.(1) is second order partial differential equation. Therefore, one initial condition and two boundary conditions are required for the solution. These boundary conditions are adopted for the center and the surface of the grain. Eq.(2) which shows the initial condition is uniform throughout the dry solid at time $t = 0$:

$$X(r,0) = X_0, \quad \text{for all } r. \quad (2)$$

The boundary conditions are

$$\frac{\partial X}{\partial r} = 0 \quad \text{for } r = 0, \quad t > 0 \quad (3)$$

$$X(R(t),t) = X_{eq}, \quad t > 0. \quad (4)$$

Eq.(3) defines symmetry of the problem in the center of the grain in any instant of time and Eq.(4) represents moisture content on the solid-fluid interface ($r = R(t)$) and it reaches equilibrium moisture content at the beginning of the soaking.

Eq.(5) represents Stefan condition representing the motion of the front. The initial condition (6) that is necessary for the solution of Eq.(5) states at the beginning of the hydration process the grain has a known radius. For soybean hydration model, $\alpha = D \frac{\rho_{DS}}{\rho_{water}}$ is obtained by Nicolin et al.[3] and R_0 is a constant.

$$\frac{dR(t)}{dt} = \alpha \frac{\partial X}{\partial r}, \quad r = R(t) \quad (5)$$

$$R(0) = R_0. \quad (6)$$

The boundary condition is defined by Eq.(3) causes an indetermination in the Eq.(1) since the Eq.(1) is not defined at the center of the grain due to term $(2/r)$ which becomes infinite when r approaches to zero. Therefore, L'Hospital rule is applied to Eq.(1) to obtain the solution for the center. Eq.(7) is valid for the center of the grain [3].

$$\frac{\partial X}{\partial t} = 3D \frac{\partial^2 X}{\partial r^2}, \quad r = 0. \quad (7)$$

3 The compact finite difference scheme

In this section, firstly, fourth and sixth order compact finite difference schemes(CFD4 and CFD6) proposed by Lele [18] are introduced. This method is particular kind of finite difference method which uses a linear combination of given values of the function on a set of points to approximate its derivatives.

Compact finite difference schemes can be dealing with two kinds of categories. These are explicit compact finite differences which compute the numerical derivatives at each grid by using large stencils and implicit compact finite differences which evaluate the numerical derivatives through solving a system of linear equation and by using the smaller stencil [19,20,21]. In this work, implicit compact finite differences for spatial discretization are used.

3.1 Spatial discretization

Spatial derivatives are computed by the compact finite difference scheme [18]. For simplicity, a uniform 1D mesh consisting of N points: $r_1 < r_2 < \dots < r_N$. The mesh size $\Delta r = r_{i+1} - r_i$ is equal at any instant of time. The first

derivatives are for all interior points (r_i, t^j) , $2 \leq i \leq N - 1$, are given by Eq.(8):

$$\alpha X'(r_{i+1}, t^j) + X'(r_i, t^j) + \alpha X'(r_{i-1}, t^j) = b \frac{X(r_{i+2}, t^j) - X(r_{i-2}, t^j)}{4\Delta r^j} + a \frac{X(r_{i+1}, t^j) - X(r_{i-1}, t^j)}{2\Delta r^j} \quad (8)$$

which provides an α -family of fourth order tridiagonal schemes with

$$a = \frac{2}{3}(\alpha + 2), \quad b = \frac{1}{3}(4\alpha - 1) \quad (9)$$

For $\alpha = \frac{1}{4}$ and $\alpha = \frac{1}{3}$ it is obtained fourth and sixth order tridiagonal schemes in Eq.(10) and Eq.(11), respectively:

$$\frac{1}{4}X'_{i-1} + X'_i + \frac{1}{4}X'_{i+1} = \frac{3}{2} \frac{X_{i+1} - X_{i-1}}{2\Delta r} \quad (10)$$

$$\frac{1}{3}X'_{i-1} + X'_i + \frac{1}{3}X'_{i+1} = \frac{1}{9} \frac{X_{i+2} - X_{i-2}}{4\Delta r} + \frac{14}{9} \frac{X_{i+1} - X_{i-1}}{2\Delta r} \quad (11)$$

where, for simplicity, X_i is taken instead of $X(r_i, t^j)$.

The derivatives of the points near the boundaries for non-periodic problems are given by one-sided schemes. The derivatives formulae at boundary points $1, 2, N - 1, N$ are given for fourth order scheme as below, respectively.

$$X'_i + 3X'_{i+1} = \frac{1}{\Delta r} \left(-\frac{17}{6}X_i + \frac{3}{2}X_{i+1} + \frac{3}{2}X_{i+2} - \frac{1}{6}X_{i+3} \right) \quad (12)$$

$$\frac{1}{4}X'_{i-1} + X'_i + \frac{1}{4}X'_{i+1} = \frac{1}{\Delta r} \left(-\frac{3}{4}X_{i-1} + \frac{3}{4}X_{i+1} \right) \quad (13)$$

$$\frac{1}{4}X'_{i-1} + X'_i + \frac{1}{4}X'_{i+1} = \frac{1}{\Delta r} \left(\frac{3}{4}X_{i+1} - \frac{3}{4}X_{i-1} \right) \quad (14)$$

$$3X'_{i-1} + X'_i = \frac{1}{\Delta r} \left(\frac{17}{6}X_i - \frac{3}{2}X_{i-1} - \frac{3}{2}X_{i-2} + \frac{1}{6}X_{i-3} \right). \quad (15)$$

Sixth order schemes formulas at boundary points $1, N$ and near the boundary points $2, N - 1$ are

$$X'_i + 5X'_{i+1} = \frac{1}{\Delta r} \left(-\frac{197}{60}X_i - \frac{5}{12}X_{i+1} + 5X_{i+2} - \frac{5}{3}X_{i+3} + \frac{5}{12}X_{i+4} - \frac{1}{20}X_{i+5} \right) \quad (16)$$

$$\frac{2}{11}X'_{i-1} + X'_i + \frac{2}{11}X'_{i+1} = \frac{1}{\Delta r} \left(-\frac{20}{33}X_{i-1} - \frac{35}{132}X_i + \frac{34}{33}X_{i+1} - \frac{7}{33}X_{i+2} + \frac{2}{33}X_{i+3} - \frac{1}{132}X_{i+4} \right) \quad (17)$$

$$\frac{2}{11}X'_{i-1} + X'_i + \frac{2}{11}X'_{i+1} = \frac{1}{\Delta r} \left(\frac{20}{33}X_{i+1} + \frac{35}{132}X_i - \frac{34}{33}X_{i-1} + \frac{7}{33}X_{i-2} - \frac{2}{33}X_{i-3} + \frac{1}{132}X_{i-4} \right) \quad (18)$$

$$5X'_{i-1} + X'_i = \frac{1}{\Delta r} \left(\frac{197}{60}X_i + \frac{5}{12}X_{i-1} - 5X_{i-2} + \frac{5}{3}X_{i-3} - \frac{5}{12}X_{i-4} + \frac{1}{20}X_{i-5} \right). \quad (19)$$

The fourth order scheme (10) with (12)-(15) can be written in the form of vector-matrix as below,

$$A_1 X' = \frac{1}{\Delta r} B_1 X$$

3.2 Application of Soybean hydration model

In numerical solution of the problem (1)-(7), three-point fourth order and sixth order compact finite difference scheme are used for derivatives of the radial coordinate where the interval is $[0, R(t)]$. Time derivatives are discretized by forward finite difference scheme.

4 Numerical algorithm

To express the volume variation Nicolin et al.[3] used Variable Space Grid method(VSGM) which was proposed Murray and Landis [22] in Eq.(1). In this method, the number of space intervals between a fixed boundary $x = 0$ and moving boundary $x = R(t)$ is kept constant and equal to N . Thus, the moving boundary lies on the N th grid. The model analyzes the time partial derivation by tracking a given line instead of a constant r . For the line i th grid point:

$$\frac{\partial X}{\partial t}|_i = \frac{\partial X}{\partial r}|_i \frac{dr}{dt}|_i + \frac{\partial X}{\partial t}|_r. \tag{20}$$

General grid point at r moves according to Eq.(21). The authors have used the method studied on Cartesian coordinates [23, 24]. Eq.(1) is in spherical coordinates but since the diffusion takes place only radial direction, mass transfer is similar to in Cartesian coordinates. Therefore, Eq.(21) can be used for this model.

$$\frac{dr_i}{dt} = \frac{r_i}{R(t)} \frac{dR(t)}{dt}. \tag{21}$$

Substituting the Eq.(20) and Eq.(21) into Eq.(1), it is obtained

$$\frac{\partial X}{\partial t} = \frac{r_i}{R(t)} \frac{dR(t)}{dt} \frac{\partial X}{\partial r} + D \left(\frac{2}{r} \frac{\partial X}{\partial r} + \frac{\partial^2 X}{\partial r^2} \right). \tag{22}$$

To solve the model the radial coordinate is divided into N points ($i = 1, 2, \dots, N$). The number of time intervals is determined by the amount of absorption water. When the whole grain reaches %99 of the equilibrium moisture content, the process is cut off.

Discretization of Eq. (2) is given by

$$X_i^1 = X_0, \quad i = 1, 2, \dots, N. \tag{23}$$

To discretization of the boundary condition which is given by Eq.(3) for the center of the grain, it is used explicit finite difference approximation:

$$X_2^j = X_0^j. \tag{24}$$

Central finite difference approximation is used in Eq.(7) which represents moisture content at the center of the grain ($r = 0$),

$$X_1^{j+1} = X_1^j + \frac{3D\Delta t}{(\Delta r^j)^2} (X_2^j - 2X_1^j + X_0^j). \tag{25}$$

To eliminate the term X_0^j it is used Eq.(24) and obtained:

$$X_1^{j+1} = X_1^j + \frac{6D\Delta t}{(\Delta r^j)^2} (X_2^j - X_1^j). \tag{26}$$

Discretization of the moisture diffusion equation for internal nodes ($2 \leq i \leq N$) is given by Eq.(27) with the position of each grid point defined by $r_i^j = (i - 1)\Delta r^j$. First and second derivatives $(X_r)_i^j$ and $(X_{rr})_i^j$ in Eq.(27), respectively, are

constructed row-by-row by using compact finite difference scheme explained above, i.e., $(X_r)_i^j = \frac{1}{\Delta r^j} A^{-1} B X_i^j$.

$$X_i^{j+1} = X_i^j + \left(\frac{\Delta t r_i^j v^j}{R^j \Delta r^j} + \frac{2D\Delta t}{r_i^j (\Delta r^j)} \right) (X_r)_i^j + \frac{D\Delta t}{(\Delta r^j)^2} (X_{rr})_i^j. \tag{27}$$

Since radial coordinate size increases with each time step due to soaking, the mesh size is defined by $\Delta r^j = R^j / N$.

The term v^j which appears in Eq.(27) represents the motion of the boundary, is the radius. The velocity of motion of the radius which is represented by Eq.(5) is discretized as

$$v^j = \left(\frac{dR}{dt} \right)^j = \frac{\rho_{DS}}{\rho_{water}} D X_{ri}^j. \tag{28}$$

The boundary condition on the spherical grain surface is presented by

$$X_N^j = X_{eq}. \tag{29}$$

The position of the radius at the next time step is calculated by the following approximation:

$$R^{j+1} = R^j + \Delta t v^j.$$

5 Numerical stability

In Section 4, it is demonstrated how compact finite difference scheme applies to soybean hydration model. If Eqs.(26), (27) and (29) are written in vector-matrix form, it yields:

$$X^{j+1} = X^j + C X^j + D X^j, \quad j = 1, 2, \dots, N-1 \tag{30}$$

where

$$C = \begin{bmatrix} -\frac{6D\Delta t}{(\Delta r^j)^2} & \frac{6D\Delta t}{(\Delta r^j)^2} & 0 & 0 & \dots & 0 \\ \alpha_2^j a_{21} & \alpha_2^j a_{22} & \alpha_2^j a_{23} & \alpha_2^j a_{24} & \dots & \alpha_2^j a_{2N} \\ \alpha_3^j a_{31} & \alpha_3^j a_{32} & \alpha_3^j a_{33} & \alpha_3^j a_{34} & \dots & \alpha_3^j a_{3N} \\ & \ddots & \ddots & \ddots & & \\ & & \ddots & \ddots & & \\ \alpha_{N-1}^j a_{N-11} & \alpha_{N-1}^j a_{N-12} & \alpha_{N-1}^j a_{N-13} & \alpha_{N-1}^j a_{N-14} & \dots & \alpha_{N-1}^j a_{N-1N} \\ 0 & 0 & 0 & 0 & \dots & 0 \end{bmatrix}$$

$$D = \begin{bmatrix} 0 & 0 & 0 & 0 & \dots & 0 \\ \beta^j b_{21} & \beta^j b_{22} & \beta^j b_{23} & \beta^j b_{24} & \dots & \beta^j b_{2N} \\ \beta^j b_{31} & \beta^j b_{32} & \beta^j b_{33} & \beta^j b_{34} & \dots & \beta^j b_{3N} \\ & \ddots & \ddots & \ddots & & \\ & & \ddots & \ddots & & \\ \beta^j b_{N-11} & \beta^j b_{N-12} & \beta^j b_{N-13} & \beta^j b_{N-14} & \dots & \beta^j b_{N-1N} \\ 0 & 0 & 0 & 0 & \dots & 0 \end{bmatrix}$$

and a_{ij} s are component of matrix $A^{-1}B$ and b_{ij} s are component of matrix $A^{-1}BA^{-1}B$. Also, $\alpha_i^j = \left(\frac{r_i^j v^j}{Rj} + \frac{2D}{r_i^j} \right) \frac{\Delta t}{\Delta r^j}$ and $\beta^j = \frac{Ddt}{(\Delta r^j)^2}$.

It is seen that the matrices C and D vary with the variable coefficients α and β . But during numerical calculation, it is observed that the coefficients do not vary rapidly and change much. As a result, the matrix properties do not change at different space and time values. For this reason, to prove the stability of the scheme the variable coefficients can be fixed at certain space and time points. Thus, the system is written at any consecutive time points as follows:

$$\begin{aligned} X^{j+1} &= (I + \gamma E + \eta F) X^j \\ &= (I + \gamma E + \eta F)^2 X^{j-1} \\ &= \dots \\ &= (I + \gamma E + \eta F)^{j+1} X^0 \end{aligned} \tag{31}$$

where, γ is the fixed α_i^j at certain space and time points and η is the fixed β^j at certain time points,

$$E = \begin{bmatrix} -\frac{6Ddt}{(\Delta r^j)^2(\gamma)} & \frac{6Ddt}{(\Delta r^j)^2(\gamma)} & 0 & 0 & \dots & 0 \\ a_{21} & a_{22} & a_{23} & a_{24} & \dots & a_{2N} \\ a_{31} & a_{32} & a_{33} & a_{34} & \dots & a_{3N} \\ & \ddots & \ddots & \ddots & & \\ & \ddots & \ddots & \ddots & & \\ a_{N-11} & a_{N-12} & a_{N-13} & a_{N-14} & \dots & a_{N-1N} \\ 0 & 0 & 0 & 0 & \dots & 0 \end{bmatrix}$$

$$F = \begin{bmatrix} 0 & 0 & 0 & 0 & \dots & 0 \\ b_{21} & b_{22} & b_{23} & b_{24} & \dots & b_{2N} \\ b_{31} & b_{32} & b_{33} & b_{34} & \dots & b_{3N} \\ & \ddots & \ddots & \ddots & & \\ & \ddots & \ddots & \ddots & & \\ b_{N-11} & b_{N-12} & b_{N-13} & b_{N-14} & \dots & b_{N-1N} \\ 0 & 0 & 0 & 0 & \dots & 0 \end{bmatrix}$$

where Δr^j in components of the first row of matrix E is determined by the same time point in α and β coefficients. According to the theory of finite difference method [25], consistent and stable finite difference method implies its convergence. For this, the magnitude of eigenvalues $(I + \lambda E + \eta F)$ must be less than or equal to 1. The eigenvalues of the matrix for different N values and different γ and η coefficients are plotted in Figure 1 and Figure 2 by calculating with MATLAB.

6 Results

The model (1)-(7) is solved by fourth and sixth compact finite difference scheme in radial coordinates and forward finite difference in time coordinates.

It is performed the computations using the software MATLAB R2012a on ASUS machine Intel Core i7 2.4 GHz 6 GB

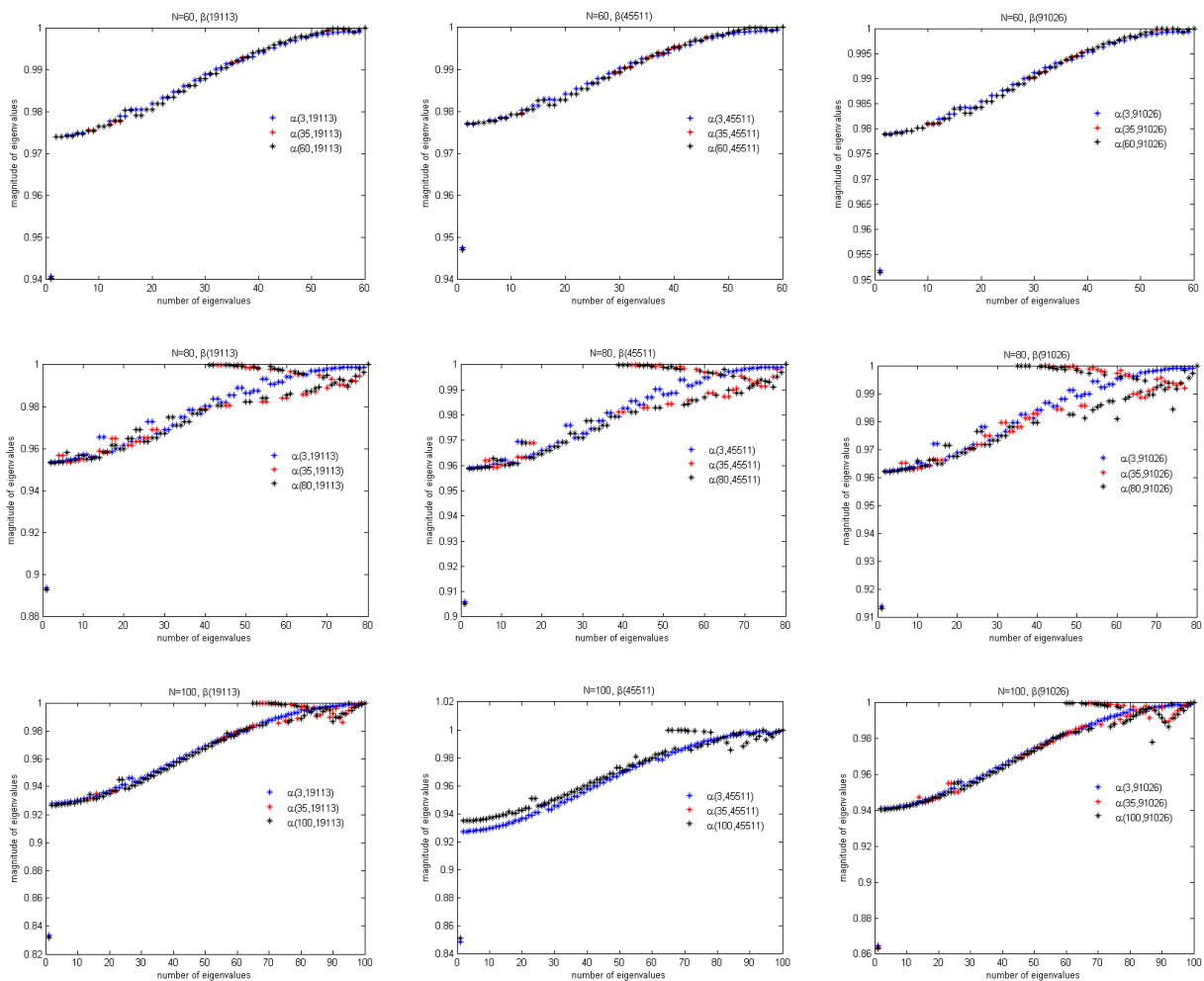


Fig. 1: Eigenvalues for CFD4 method for different α and β values at values of $N = 60, 80$ and 100 .

memory. The computational domain for space is considered $0 \leq r \leq R(t)$, is evaluated by over time and different numbers of uniform mesh point are used for numerical calculations.

Constants in the model [3, 26] are given as below:

$D \times 10^{-11} (m^2/s)$	$\rho_{DS} (kg_{DS}/m^3)$	$\rho_{water} (kg_{water}/m^3)$	$X_{eq} (kg_{water}/kg_{DS})$	$X_0 (kg_{water}/kg_{DS})$	$R_0 (m)$
3.277	1.057	1.000	1.651	0.126	0.003

The correct choice of the number of spatial points (r) is essential for adequate representation of the numerical solutions. While a small number of divisions of spatial coordinate may lead to non-realistic approximations due to rounding error, the profiles are obtained by simulation with an extremely large number of divisions are impracticable due to processing time. The best way is for determining the smallest number of discretization points that could preserve the representability of numerical solution of the mathematical model.

As a numerical experiment, it is experimented the model for N values between 10 and 50. Figure 3 shows moisture

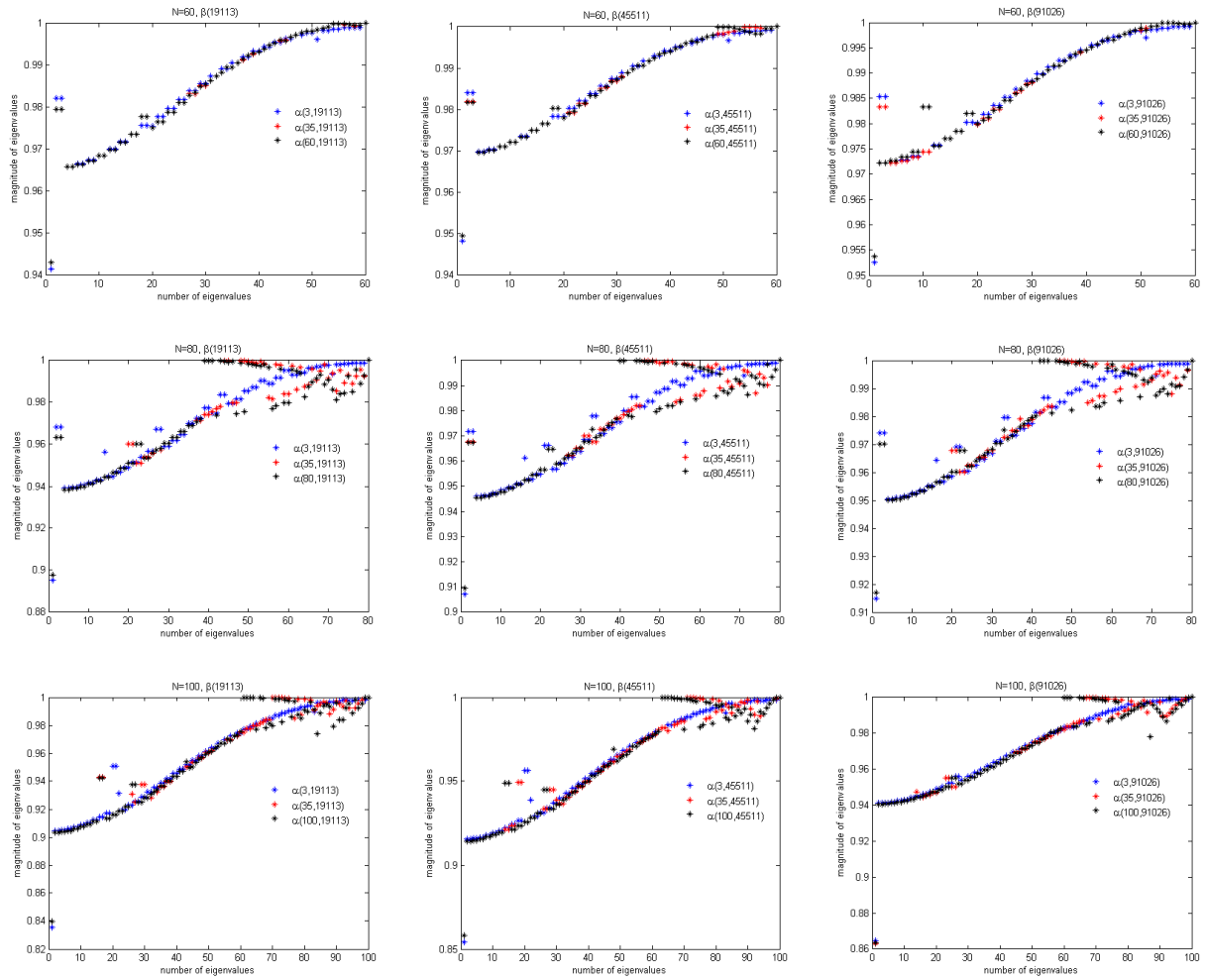


Fig. 2: Eigenvalues for CFD6 method for different α and β values at values of $N = 60, 80$ and 100 .

content values as a function of the radius for various values of time are obtained for extreme two N values (for $N = 10$ and $N = 50$) by using CFD4 and CFD6. As is seen, the greatest moisture content variations occur near the surface at the beginning of the soaking and oscillations occur at small times (approximately around 5000 s). The calculations with these values do not show realistic numerical solutions when compared to the results that Nicolin et al.[3] validated with experimental data. However, the results obtained with values of $60 \leq N \leq 100$ show a realistic approach. If N values larger than 100, as mentioned above, CPU times increase (see Table 5). When we run the problem extremely large N values such as $307 \leq N \leq 334$ the obtained equilibrium time diverges from the experimental equilibrium time for CFD4. When $N \geq 335$ CFD4 solutions and $N \geq 280$ CFD6 solutions are degenerated, see Figure 4. Figure 5 shows moisture profiles as a function of the radius for various values of time and Figure 6 shows moisture profiles as a function of time for various values of the radius.

To compare the numerical solutions which are obtained in this work with experimental moisture content data in Ref. [27] the mean values for the models are averaged over the volume grain by using Eq.(32),

$$X_m = \frac{\int_0^R X \cdot r^2 dr}{\int_0^R r^2 dr} \quad (32)$$

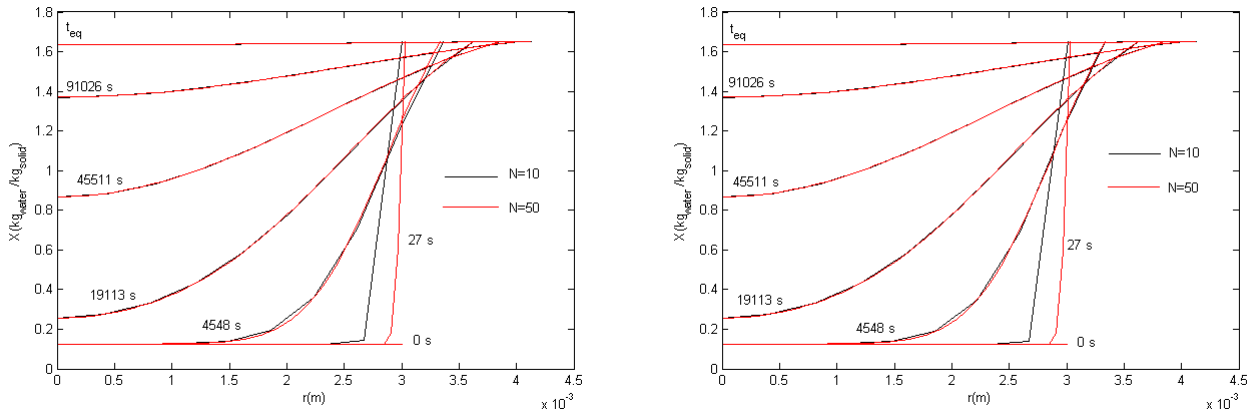


Fig. 3: Solutions of the model as a function of the radius by CFD4 (left) and CFD6 (right) for $N = 10$ and $N = 50$.

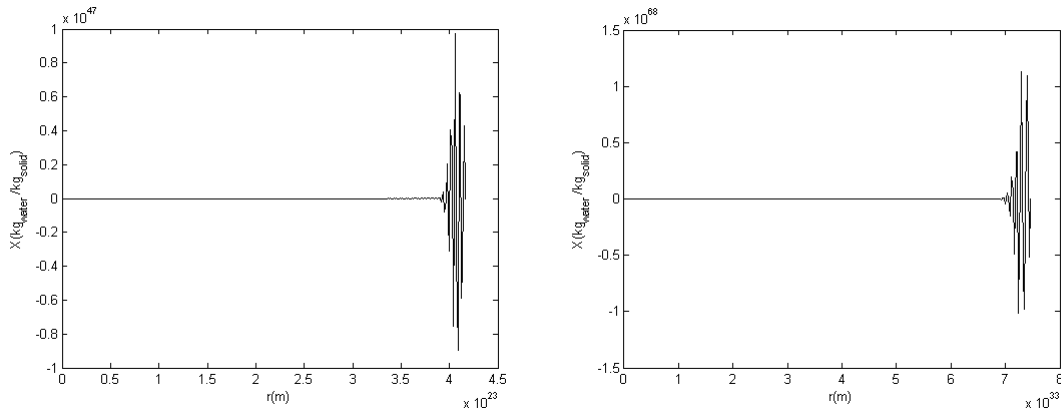


Fig. 4: Solutions of the model as a function of the radius by CFD4 (left) and CFD6 (right) for $N = 335$ and $N = 280$.

and in Figure 7, the average profiles are compared with experimental moisture content data. On the other hand, mean squared errors calculated by Eq.(33) between numerical solution and experimental moisture content data are listed in Table 1. Mean squared errors show that the experimental data and numerical solutions are in good agreement.

$$MSE = \frac{1}{n} \sum_{i=1}^n (\hat{X}_i - X_{mi})^2 \tag{33}$$

where n is number of data, \hat{X} is the experimental data and X_m is the average moisture content is calculated by Eq.(32).

Table 1: Mean squared errors for different N values.

	Nicolin et al.[3]	CFD4	CFD6
N	$MSE \times 10^3$	$MSE \times 10^3$	$MSE \times 10^3$
60	1.927796	1.993219	1.986565
80	1.951536	1.988650	1.985040
100	1.963276	1.988205	1.987798

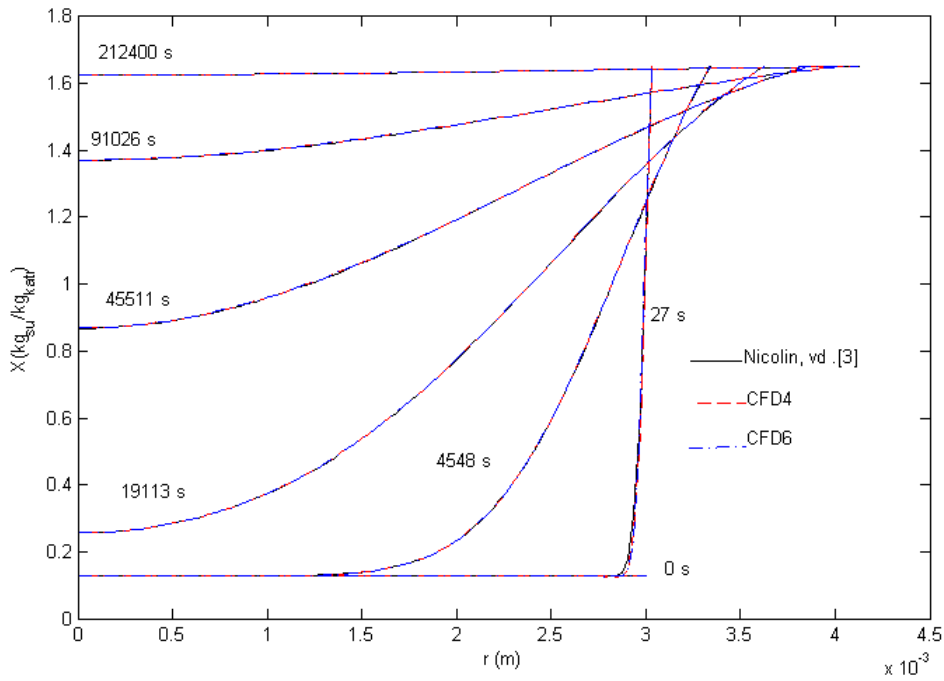


Fig. 5: Solutions of the model as a function of the radius by Nicolin et al. [3], CFD4 and CFD6 for $N = 100$ at various times.

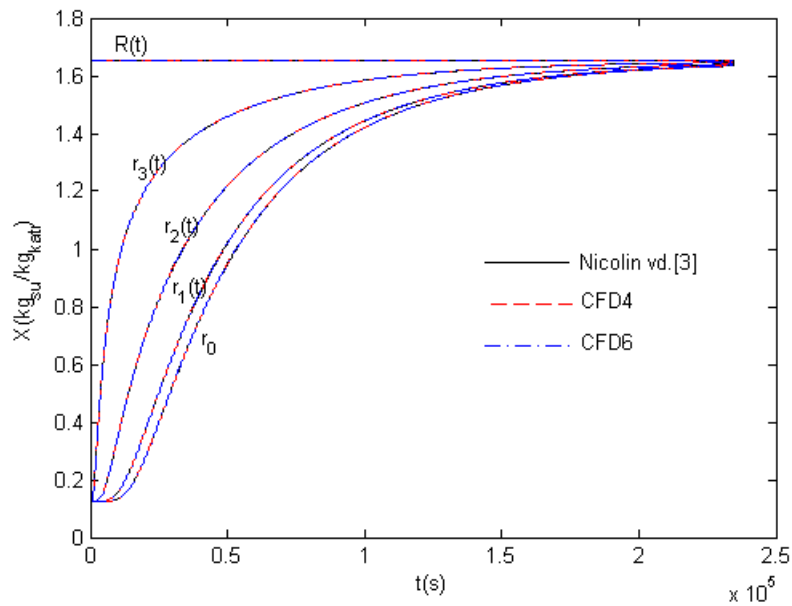


Fig. 6: Solutions of the model as a function of time by Nicolin et al.[3], CFD4 and CFD6 for $N = 100$ at various the radius.

Also, absolute errors and relative errors which are listed in Table 2 are calculated as in below, respectively:

$$e = |X_t^{j+1} - X_t^j| \tag{34}$$

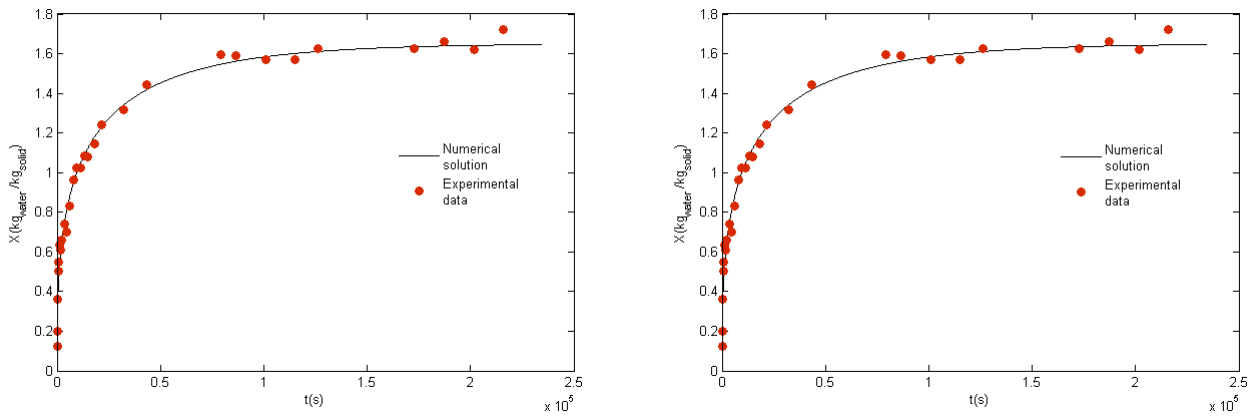


Fig. 7: Comparison of experimental data and numerical solution by obtained CFD4 (left) and CFD6 (right).

$$\eta = \frac{\epsilon}{X_i^j} \tag{35}$$

Errors of three methods which are calculated with different N values are very close to each other. The values calculated for $N = 100$ are given in Table 2.

Table 2: Absolute and Relative Error at different times for $N = 100$.

		Nicolin et al.[3]		CFD4		CFD6	
$r(m)$	$t(s)$	Absolute Error	Relative Error	Absolute Error	Relative Error	Absolute Error	Relative Error
0.001	27	0.0	0.0	0.0	0.0	2.775557e-17	2.202823e-16
	4548	1.390885e-06	1.096337e-05	1.352781e-06	1.066619e-05	1.352473	1.066382e-05
	19113	2.713013e-05	7.128857e-05	2.717108e-05	7.137700e-05	2.717115e-05	7.137799e-05
	45511	1.656995e-05	1.724013e-05	1.657417e-05	1.723278e-05	1.657425e-05	1.723289e-05
	91026	5.302804e-06	3.784680e-06	5.297441e-06	3.779458e-06	5.297453e-06	3.779467e-06
	t_{eq}	2.851582e-07	1.742971e-07	2.855206e-07	1.745186e-07	2.855201e-07	1.745183e-07
	0.002	27	0.0	0.0	2.013140e-12	1.597730e-11	1.040613e-09
4548		5.543744e-05	2.414386e-04	5.548694e-05	2.424036e-04	5.548642e-05	2.424134e-04
19113		2.844106e-05	3.635749e-05	2.846550e-05	3.637864e-05	2.846574e-05	3.637913e-05
45511		1.125378e-05	9.469479e-06	1.125424e-05	9.466270e-06	1.125428e-05	9.466319e-06
91026		3.666935e-06	2.485237e-06	3.663415e-06	2.482251e-06	3.663423e-06	2.482257e-06
t_{eq}		2.058661e-07	1.255135e-07	2.061279e-07	1.256731e-07	2.061277e-07	1.256729e-07
0.003		27	0.010978	0.009780	0.010615	0.009662	0.011113
	4548	5.239481e-05	4.192512e-05	5.257732e-05	4.208453e-05	5.258039e-05	4.208723e-05
	19113	1.130235e-05	8.318473e-06	1.130781e-05	8.321875e-06	1.130790e-05	8.321951e-06
	45511	4.424064e-06	3.018096e-06	4.423744e-06	3.017512e-06	4.423762e-06	3.017525e-06
	91026	1.636938e-06	1.042253e-06	1.635525e-06	1.041248e-06	1.635528e-06	1.041250e-06
	t_{eq}	9.916444e-08	6.025364e-08	9.929071e-08	6.033036e-08	9.929056e-08	6.033027e-08

Table 3 shows the position of the radius and its velocity for Nicolin et al. [3], CFD4 method and CFD6 method at different time values and different N values. In Figure 8, the increase in the size of the grain is shown. Nicolin et al. [3] demonstrated numerically R_{max} has $\approx 37.4\%$ and experimentally $\approx 40.6\%$ the increasing. In the calculations of this work, the increase in the radius $\%37.47$ for both method, CFD4 and CFD6. Hence, the results are obtained by CFD4 and CFD6 schemes approximate the result of Nicolin et al. [3] very well.

Table 3: Comparison of the position of the radius and velocity of the radius at different times for different N values.

N	$t(s)$	Position of Radius			Velocity of Radius		
		Nicolin et al.[3]	CFD4	CFD6	Nicolin et al.[3]	CFD4	CFD6
60	27	0.003027	0.003032	0.003034	7.188910e-07	6.581855e-07	5.210668e-07
	4548	0.003341	0.003337	0.003337	3.347523e-08	3.352256e-08	3.352582e-08
	19113	0.003626	0.003623	0.003623	1.283695e-08	1.284040e-08	1.284044e-08
	45511	0.003854	0.003851	0.003851	5.888267e-09	5.885257e-09	5.885261e-09
	91026	0.004023	0.004019	0.004019	2.206632e-09	2.202524e-09	2.202519e-09
	t_{eq}	0.004129	0.004124	0.004124	1.377649e-10	1.378431e-10	1.378416e-10
80	27	0.003029	0.003031	0.003030	6.479504e-07	4.585342e-07	3.246622e-07
	4548	0.003340	0.003337	0.003337	3.347523e-08	3.352446e-08	3.352675e-08
	19113	0.003626	0.003623	0.003623	1.283695e-08	1.284037e-08	1.284044e-08
	45511	0.003854	0.003851	0.003851	5.888267e-09	5.885222e-09	5.885234e-09
	91026	0.004023	0.004019	0.004019	2.206632e-09	2.202490e-09	2.202491e-09
	t_{eq}	0.004129	0.004124	0.004124	1.377649e-10	1.378418e-10	1.378439e-10
100	27	0.003029	0.003029	0.003027	5.882738e-07	4.082022e-07	3.717675e-07
	4548	0.003339	0.003337	0.003337	3.349053e-08	3.352564e-08	3.352743e-08
	19113	0.003625	0.003623	0.003623	1.283846e-08	1.284039e-08	1.2840473e-08
	45511	0.003853	0.003851	0.003851	5.887775e-09	5.885213e-09	5.885230e-09
	91026	0.004021	0.004019	0.004019	2.205708e-09	2.202477e-09	2.202480e-09
	t_{eq}	0.004127	0.004124	0.004124	1.377806e-10	1.378441e-10	1.378438e-10

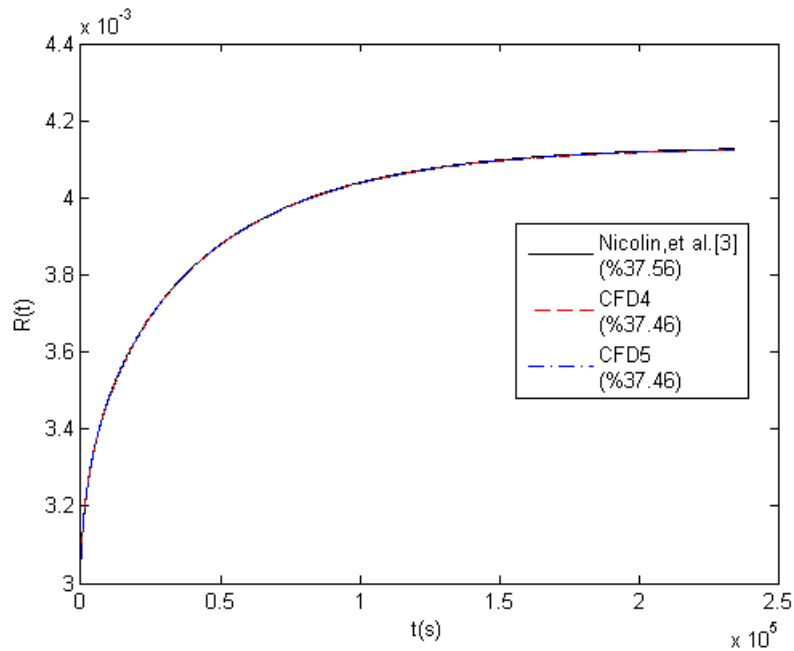


Fig. 8: Grain radius is calculated by Nicolin et al. [3], CFD4 and CFD6 for $N = 100$.

To show accuracy of the methods convergence rates are calculated by

$$r = \log \left(\frac{X_{\Delta r} - X_{\Delta r/2}}{X_{\Delta r/2} - X_{\Delta r/4}} \right) / \log 2.$$

From the results in Table 4, although error order of CFD4 and CFD6 do not behave as $O(h^4)$ and $O(h^6)$, respectively, CFD4 and CFD6 are more accurate than Nicolin et al. [3].

Equilibrium time (t_{eq}) is defined the time at which the center of the grain reaches 99% of the equilibrium moisture content.

Table 4: Convergence results for Nicolin et al. [3], CFD4 and CFD6.

Nicolin et al. [3]				CFD4				CFD6			
t	Δr	$\max(X_{\Delta r} - X_{\Delta r/2})$	$\frac{X_{\Delta r} - X_{\Delta r/2}}{X_{\Delta r/2} - X_{\Delta r/4}}$	Convergence rate	$\max(X_{\Delta r} - X_{\Delta r/2})$	$\frac{X_{\Delta r} - X_{\Delta r/2}}{X_{\Delta r/2} - X_{\Delta r/4}}$	Convergence rate	$\max(X_{\Delta r} - X_{\Delta r/2})$	$\frac{X_{\Delta r} - X_{\Delta r/2}}{X_{\Delta r/2} - X_{\Delta r/4}}$	Convergence rate	
19113	1/10	0.014464	3.574730	1.837834	0.001727	8.145801	3.026056	0.001219	7.085736	2.824917	
	1/20	0.004046	4.159013	2.056241	2.121289e-04	7.899908	2.981835	1.721430e-04	7.79285	2.96621525	
	1/40	9.728773e-04	4.159013	2.339704	2.685207e-05	5.920900	2.565816	2.208985e-05	2.614956	1.386787	
	1/80	1.921927e-04	-	-	4.535133e-06	-	-	8.447501e-06	-	-	
	1/160	-	-	-	-	-	-	-	-	-	
45511	1/10	0.002895	1.930698	0.949122	0.001831	6.866960	2.779671	0.001623	6.947927	2.796582	
	1/20	0.001499	1.926042	0.945639	2.666580e-04	6.653554	2.734125	2.336222e-04	6.782086	2.761729	
	1/40	7.787053e-04	2.081232	1.057437	4.007752e-05	8.807606	3.138750	3.444695e-05	18.809912	4.233420	
	1/80	3.741559e-04	-	-	4.550331e-06	-	-	1.831319e-06	-	-	
	1/160	-	-	-	-	-	-	-	-	-	
91026	1/10	0.006976	2.839293	1.505532	0.001125	6.735154	2.751711	9.521441e-04	6.677889	2.739391	
	1/20	0.002457	2.653240	1.407755	1.671038e-04	6.298509	2.655010	1.425816e-04	6.350026	2.666762	
	1/40	9.260486e-04	2.564316	1.358574	2.653069e-05	4.906602	2.294724	2.245370e-05	5.006112	2.323690	
	1/80	3.611288e-04	-	-	5.407141e-06	-	-	4.485257e-06	-	-	
	1/160	-	-	-	-	-	-	-	-	-	
t_{eq}	1/10	0.001381	3.063930	1.615383	1.399843e-04	6.390913	2.676022	1.202204e-04	6.458128	2.691116	
	1/20	4.509273e-04	2.845108	1.508483	2.190365e-05	6.057103	2.598628	1.861256e-05	6.077461	2.603468	
	1/40	1.584921e-04	2.717706	1.442389	3.616192e-06	3.876006	1.954570	3.062555e-06	3.469529	3.469528	
	1/80	5.831834e-05	-	-	9.329687e-07	-	-	8.827005e-07	-	-	
	1/160	-	-	-	-	-	-	-	-	-	

In Table 5, the equilibrium time is listed for three methods and it is shown that t_{eq} is shorter than Nicolin et al. [3] but are realistic with less iteration. Also, CPU times at different N values for all the methods are given in Table 5 and these are shorter than Nicolin et al. [3] for all N values.

Table 5: Equilibrium times and CPU times for different N values.

N	Nicolin et al.[3]		CFD4		CFD6	
	t_{eq}	CPU	t_{eq}	CPU	t_{eq}	CPU
60	234662	293.124552	234148	96.316208	234148	10.052013
80	234507	329.169541	234146	120.966301	234145	18.794400
100	234423	368.56395	234144	125.140448	234144	22.644993.

7 Conclusion

In this paper, fourth and sixth order compact finite difference schemes are used for soybean hydration model. It is worth to mention that the compact finite difference scheme utilized for this problem is always stable since the modulus of the spectral radius of iteration matrix is always 1. On the other hand, the number $rate = \log \left(\frac{X_{\Delta r} - X_{\Delta r/2}}{X_{\Delta r/2} - X_{\Delta r/4}} \right)$ provides a measure for the comparison of the rate of convergence of different iterative methods when N is sufficiently large, so, the obtained results confirm that our approach is asymptotically convergent and this also an indication that the number of iteration is required to reduce the error for sufficiently large N . For this reason, the solutions are obtained by fourth and sixth order compact finite differences are compatible to the available solutions in the literature and our approach reaches equilibrium time with less iteration with minimal computational effort (CPU time).

Competing interests

The authors declare that they have no competing interests.

Authors' contributions

All authors have contributed to all parts of the article. All authors read and approved the final manuscript.

References

- [1] M. R. Coutinho, Modeling, Simulation and Analysis of the Hydration of Soy Beans, Thesis (Doctorate in Chemical Engineering), State University of Maringá, Brazil (2006).
- [2] D. J. Nicolin, M.R.Coutinho, C.M.G.Andrade, L. M. M. Jorge, Hsu model analysis considering grain volume variation during soybean hydration, *J. Food Eng.*, 111 (2012) 496-504.
- [3] D. J. Nicolin, R. M. M. Jorge, L. M. M. Jorge, Moving boundary modeling of conventional and transgenic soybean hydration: Moisture profile and moving front experimental validation, *J. Heat Mass Trans.* 90 (2015) 568-567.
- [4] M.J.Davey, K.A.Landman, M.J.McGuinness, H.N.Jin, Mathematical modeling of rice cooking and dissolution in beer production, *AIChE J.* 48 (2002) 1811-1826.
- [5] M.J.McGuinness, C.P.Please, N. Fowkes, P. McGowan, L. Ryder, D. Forte, Modelling the wetting and cooking of a single cereal grain, *IMA J. Manage Math.* 11 (2000) 49-70.
- [6] S.I.Barry, J. Counce, Exact and numerical solutions to a Stefan problem with two moving boundaries, *Appl. Math. Model.* 32 (2008) 83-98.
- [7] M. R. Coutinho, W. A. dos S. Conceição, P. R. Paraiso, C. M. G. Andrade, E. S. Jorge, R. Filho Maciel, L. M. M. Jorge, Application of the Hsu model to soybean grain hydration, *Food. Sci Technol.* 30 (2010) 19-29.
- [8] D. J. Nicolin, M. R. Coutinho, C. M. G. Andrade, L. M. M. Jorge, Soybean Hydration: Investigation of Distributed Parameter Models with Respect to Surface Boundary Conditions, *Chem. Eng. Comm.* 200 (2013) 959-976.
- [9] J. Crank, *Free and Moving Boundary Problems*, Clarendon Press, Oxford, 1984.
- [10] N. Sadoun, E.K.Si-Ahmed, J. Legrand, On Heat Conduction with Phase Change: Accurate Explicit Numerical Method, *J. Appl. Fluid Mech.* 5 (2012) 105-112.
- [11] F. Yiğit, One-dimensional solidification of pure materials with a time periodically oscillating temperature boundary condition, *Appl. Math. Comput.* 217 (2011) 6541-6555.
- [12] S.Y.Reutskiy, A meshless method for one-dimensional Stefan problems, *Appl. Math. Comput.* 217 (2011) 9689-9701.
- [13] S.Y.Reutskiy, The method of approximate fundamental solutions (MAFS) for Stefan problems for the sphere, *Appl. Math. Comput.* 227 (2014) 648-655.
- [14] S. L. Mitchell, M. Vynnycky, I. G. Gusev, S. S. Sazhin, An accurate numerical solution for the transient heating of an evaporating spherical droplet, *Appl. Math. Comput.* 217 (2011) 9219-9233.
- [15] T. E. Lee, M. J. Baines, S. Langdon, A finite difference moving mesh method based on conservation for moving boundary problems, *J. Comput. Appl. Mathematics*, 288 (2015) 1-17.
- [16] P.E. Viollaz, C.O. Rovedo, C.Suarez, Numerical treatment of transient diffusion in shrinking or swelling solids, *Int. Commun. Heat Mass Transfer* 22 (1995) 527-538.
- [17] P.E. Viollaz, C.O. Rovedo, A drying model for three-dimensional shrinking bodies, *J. Food Eng.* 52 (2002) 149-153.
- [18] S. K. Lele, Compact Finite Difference Schemes with Spectral-like Resolution, *J. Comput. Physics*, 103 (1992) 16-42.
- [19] J.Li, J.Li, High-Order compact difference methods for simulating wave propagations in excitable media, *J. Num. Anal. Model.* 5 (2014) 339-346.
- [20] J.Li, Y.Chen, G.Liu, High-Order Compact ADI Methods for Parabolic Equations, *Comput. Math. Appl.* 52 (2006) 1343-1356.
- [21] M. Sarı, G. Gürarlan, A sixth-order compact finite difference scheme to the numerical solutions of Burgers' equation, *Appl. Math. Comput.* 208 (2009) 475-483.
- [22] W. D. Murray, F. Landis, Numerical and machine solutions of transient heat-conduction problems involving melting or freezing, *J. Heat Transfer* 81 (1959) 106-112.
- [23] N. Sadoun, E.K.Si-Ahmed, J. Legrand, On Heat Conduction with Phase Change: Accurate Explicit Numerical Method, *J. Appl. Fluid Mech.* 5 (2012) 105-112.
- [24] S. Kutluay, A. R. Bahadır, A. Ozdes, The numerical solution of one-phase classical Stefan problem, *J. Comput. Appl. Math.* 81 (1997) 135-144.
- [25] J. C. Strikwerda, *Finite Difference Schemes and Partial Differential Equations*, Chapman & Hall, New York, 1989.
- [26] D. J. Nicolin, E. C. da S. Gisleine, R. M. M. Jorge, L. M. M. Jorge, Numerical Solution of a Nonlinear Diffusion Model for Soybean Hydration with Moving Boundary, *Int. J. Food Eng.* 5 (2015) 587-595.
- [27] D. J. Nicolin, *Investigação de Modelos Fenológicos Aplicados a Hidratada de Soja Convencional e Transgênica*, Universidade Estadual de Maringá-PR Brazil, (2015), 144pp.